Measurement of the Reaction $\gamma\gamma \to \pi^+\pi^+\pi^-\pi^-$ at PETRA

CELLO Collaboration

H.-J. Behrend, H. Fenner, M.-J. Schachter[1], V. Schröder, H. Sindt

Deutsches Elektronen-Synchrotron, DESY, D-2000 Hamburg, Federal Republic of Germany

O. Achterberg, G. D'Agostini, W.-D. Apel, J. Engler, G. Flügge, B. Forstbauer, D.C. Fries,
W. Fues, K. Gamerdinger, Th. Henkes, G. Hopp, M. Krüger, H. Küster, H. Müller, H. Randoll[2],
G. Schmidt[3], H. Schneider

Kernforschungszentrum Karlsruhe and Universität Karlsruhe, D-7500 Karlsruhe, Federal Republic of Germany

W. de Boer, G. Buschhorn, G. Grindhammer, P. Grosse-Wiesmann, B. Gunderson, C. Kiesling,
R. Kotthaus, U. Kruse[4], H. Lierl, D. Lüers, H. Oberlack, P. Schacht

Max-Planck-Institut für Physik und Astrophysik, D-8000 München, Federal Republic of Germany

G. Bonneaud[5], P. Colas, A. Cordier, M. Davier, D. Fournier, J.F. Grivaz, J. Haissinski,
V. Journé, F. Laplanche, F. Le Diberder, U. Mallik[6], E. Ros, J.-J. Veillet

Laboratoire de l'Accélérateur Linéaire, F-91405 Orsay, France

J.H. Field[7], R. George, M. Goldberg, B. Grossetête, O. Hamon, F. Kapusta,
F. Kovacs, G. London, R. Pain, L. Poggioli, M. Rivoal

Laboratoire de la Physique Nucléaire et Hautes Energies, Université de Paris, F-75230 Paris, France

R. Aleksan, J. Bouchez, G. Carnesecchi, G. Cozzika, Y. Ducros, A. Gaidot,
P. Jarry, Y. Lavagne, J. Pamela, J.P. Pansart, F. Pierre

Centre d'Etudes Nucléaires, Saclay, F-91190 Gif-sur-Yvette, France

Received 7 September 1983

Abstract. We have determined the cross section for $\gamma\gamma \to \pi^+\pi^+\pi^-\pi^-$ in a way free of assumptions about the relative contributions from $\rho^0\rho^0$, $\rho^0 2\pi$ and 4π (uncorrelated phase space). We find a sharp onset above threshold and a rather high cross section of about 200 nb around $W_{\gamma\gamma} = 1.5$ GeV which consists to about 40% of $\rho^0\rho^0$ production with sizeable contributions from $\rho^0 2\pi$ and 4π (PS). The total cross section as well as the $\rho^0\rho^0$ content fall rather fast at higher c.m. energies. Attempts to explain this be-
haviour in terms of production of known resonances are not successful so far. The angular distributions do not show any significant structure pointing to resonance formation in the 4π-system. Only the ρ^0-meson is observed in the moment analysis. The decay distributions of the ρ^0 for forward produced rhos are fairly consistent with helicity conservation of the produced rhos in accordance with the VDM picture.

1 Now at SCS, Hamburg, FRG
2 Now at Blaupunkt, Hildesheim, FRG
3 Now at Siemens, München, FRG
4 Now at University of Illinois, Urbana, USA
5 Now at CRN Strasbourg, France
6 Now at University of Purdue, Purdue, USA
7 On leave of absence from DESY, Hamburg, FRG

1. Introduction

Since higher energies became available at electron positron colliders (PETRA, PEP), the interest in photon photon collisions has increased considerably.

These processes offer the possibility to study the formation and decay of $C = +1$ resonant states and to compare the results with predictions from different models (VDM, quark parton etc.). For a clear identification of the process

$$e^+e^- \to e^+e^- + \gamma\gamma \to e^+e^- + \pi^+\pi^+\pi^-\pi^- \tag{1}$$

one has to detect at least one of the scattered electrons with small angle tagging systems in addition to detecting the hadronic final state. This has the disadvantage that the event rate is considerably reduced since the directional distribution of the bremsstrahlung quanta radiated off the electron (positron) is sharply forward peaked. Present day techniques and luminosities only allow the study of these reactions if one integrates over all hadronic final states (inelastic $\gamma\gamma$ scattering).

For the kinematical separation of reaction (1) without tagging an electron, one uses the fact that the vast majority of events are due to γ quanta which are radiated close to $0°$ with respect to the beams. Events with unobserved hadrons are eliminated by a cut in the total transverse momentum while 1γ annihilation events of the type $e^+e^- \to \gamma \to$ hadrons can be easily separated on the basis of the total visible energy spectrum. Due to the bremsstrahlung nature of the parent γ's, events from process (1) have a total hadronic energy of $\lesssim 1$–2 GeV/c.

Reaction (1) has been studied by the TASSO group [1] at PETRA and the MARK II group at SPEAR [2]. Both groups find a cross section which peaks around a center of mass energy of 1.5 GeV falling sharply towards higher energies. Most, if not all, of the events were consistent with the assumption $\gamma\gamma \to \rho^0\rho^0$. Since the measured cross section was found to be considerably larger than predicted by the VDM model, several authors have tried to explain the data by assuming resonances close to 1.5 GeV decaying into two rhos [3].

The aim of this experiment is threefold:
- measurement of the total 4π-cross section as a function of the c.m. energy of the $\gamma\gamma$ system between 1.1 and 2.5 GeV in order to study the possible formation of resonances,
- determination of the relative contributions of $\rho^0\rho^0$, $\rho 2\pi$ and uncorrelated 4π (PS = phase space distributed) to the total cross section,
- study of the angular distributions of the "ρ^0" in the overall c.m. system and of the decay π^+ of a "ρ^0" in the appropriate rest system of its parent, where we call "ρ^0" any possible $\pi^+\pi^-$-state with a mass not too far away from the known ρ^0 mass.

The difference to the previous experiments is the following:

- angular coverage in the polar angle θ goes up to $|\cos\theta| = 0.94$,
- trigger acceptance is higher due to a trigger demanding only two charged particles without angular bias up to $|\cos\theta| = 0.89$,
- a good coverage with shower counters to reject events with additional neutrals.

2. Detector Description and Data Selection

The experiment was performed using the CELLO detector at PETRA at an average beam energy of 17 GeV with a total integrated luminosity of $11.2\,\mathrm{nb}^{-1}$. The detector has been described previously [4].

The essential detector part for this experiment has been the central track detector consisting of 7 drift chambers and 5 multiwire proportional chambers in a cylindrical geometry which were operated in a $1.3\,T$ axial magnetic field. For the momentum resolution of the chamber system we achieved $\sigma(p)/p = 0.015 \cdot \sqrt{1.0 + p^2}\,[\mathrm{GeV}^2]$, except for forward-going particles which traverse only part of the chamber system.

Surrounding the track detector, a cylindrical lead-liquid argon calorimeter detected showers from charged and neutral particles. This system covered 86% of the solid angle. Each of 16 calorimeter modules sampled the energy deposited in the liquid argon 17 times in depth. We obtained an energy resolution of $\sigma(E)/E = 13\%/\sqrt{E}$ (E in GeV) with an angular resolution of 4 mrad. The particle tracks determined in the central detector were extrapolated into the calorimeter. Additional showers were defined as those which could not be linked to the charged particle tracks.

The data acquisition was triggered if at least 2 charged particles separated by more than about $6°$ in a plane perpendicular to the beam ($R\phi$ plane) were discovered in coincidence with at least one charged particle track in a plane containing the beam axis (Rz plane). The trigger decision was done, without dead time, in a fast, programmable RAM-unit, demanding, in the $R\phi$ plane, 5 of a possible 7 central detector chamber hits in a configuration corresponding to the track of a charged particle with more than 200 MeV/c, and in Rz, from 5 cylindrical layers of cathode strips, 4 hits lying in a line containing the intersection point within ± 10 cm.

The track analysis selected events using the following criteria:
- 4 charged particles with net charge zero,
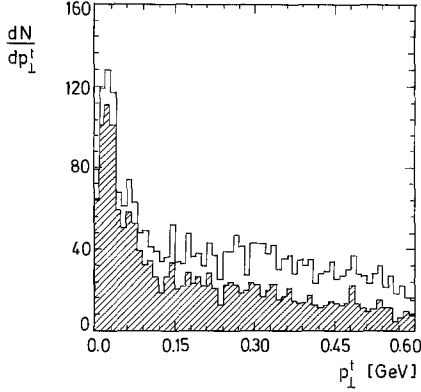- momentum of each particle above 120 MeV/c,

Fig. 1. The total transverse momentum distribution $p_\perp^t = \sum \mathbf{p}_\perp^i$. The upper histogram represents the result for all events (dataset A), the shaded histogram describes the distribution of events where all those with additional photons with energies greater than 100 MeV are removed (dataset B)

- at least 5 hits required from a total of 12 chambers allowing for tracks with a minimum polar angle of 18°,
- pairs created in the beam pipe were removed by demanding an included angle between any two particles of at least 200 mrad,
- tracks had to originate from a nominal vertex within ± 1 cm in the $R\phi$ plane and ± 4 cm in the Rz plane.

The selected events were subjected to a simultaneous fit of all tracks, using the known vertex point, which was measured separately for each storage ring filling using Bhabha events. On Fig. 1 we plot the total transverse momentum distribution with respect to the beam axis

$$p_\perp^t = \left| \sum_{i=1}^{4} \mathbf{p}_\perp^i \right|.$$

The peak at low $p_\perp^t$ contains the candidates of reaction (1). It should be noted that a visual scan of part of the data did not reduce the data sample any further. For the subsequent analysis all events with $p_\perp^t < 120$ MeV/c were collected and called dataset A.

In a further reduction step, we removed all events with additional showers corresponding to an energy deposit of at least 100 MeV in the central liquid argon calorimeter (dataset B). The resulting $p_\perp^t$-distribution is also shown in Fig. 1. The background in the higher $p_\perp^t$-region is considerably reduced. Since this procedure also cuts into the desired signal in an unknown way due to showers faked by electronic noise, no attempt was made to extract the cross section for reaction (1) from datset B. It was, however, extensively used for fits determining the different reaction channels and the angular analysis.

The final dataset A consisted of 910 events with $m(\pi\pi) < 1.5$ GeV and $1.1 < W_{\gamma\gamma} < 2.5$ GeV. Here $m(\pi\pi)$ is the effective mass of any combination of 2 unlike-sign particles in the event and $W_{\gamma\gamma}$ is the c.m. energy of the 4π system.

The $p_\perp^t$-distribution of dataset A was fitted to the superposition of a Monte Carlo simulation of reaction (1), using the exact cross section for transverse photons [5], and a polynomial background term. The generator has been compared in detail with the exact Feynman diagram calculation by Vermaseren [6]. This comparison showed that longitudinal photons contribute only at the few percent level and can be neglected to a good approximation for untagged reactions. The generated events were sent through the detector simulation and subjected to the same cuts as the real data.

For the background, we can make the plausible assumption that its density in a $p_x^t - p_y^t$-scatter plot (p_x^t, p_y^t are the horizontal, vertical components of $p_\perp^t$) is constant near $p_\perp^t = 0$. For small $p_\perp^t$ the background changes linearly with the phase space, and the phase space depends quadratically on $p_\perp^t$. So, for the description of the background, a polynomial with terms up to 8th degree without a constant or a linear term was used.

The sum of the two components described the experimental distribution well ($\chi^2/\text{D.F.} = 102/91$). We found a 9% background contribution in the event sample below a $p_\perp^t$-cut of 120 MeV/c and a loss of 14% for events due to reaction (1) above the cut.

No attempt was made to discriminate against charged K-mesons. A possible K-contamination in the total cross section cannot be ruled out. TASSO [1] however has found that this is negligible.

3. The Total Cross Section $\gamma\gamma \to \pi^+\pi^+\pi^-\pi^-$

a) Description of the Method

The acceptance of reaction (1) depends critically on the momentum distribution of the produced pions which depends on the following factors:

- For a fixed $W_{\gamma\gamma}$ the differential cross section depends on the $E_{\gamma 1} - E_{\gamma 2}$-distribution, which has been calculated and included in the Monte Carlo simulation.
- If two or three pions or both pairs of pions form a resonance, the differential cross section depends on the mass distribution of the resonance.
- In the case of resonance production, the differential cross section depends on the production and decay angular distributions.

Previous experiments have seen a clear ρ^0 signal when the invariant masses of the unlike-sign com-

binations were plotted [1, 2]. This is in good agreement also with our data. On the other hand, TASSO [1] finds also sizeable contributions from 4π phase space and $\rho 2\pi$ depending on the method they use for the fit. Monte Carlo studies show that the acceptances for $\gamma\gamma\to\rho\rho$ and for $\gamma\gamma\to 4\pi$ (PS) differ by almost a factor of 2. Other resonances (for example A_1) have been seen neither in the previous experiments nor in this one. We, therefore, assume, in the following, that either 0, 1 or 2 ρ^0 mesons are formed and that the other π's are distributed according to phase space.

In order to arrive at a cross section which is independent of the ρ^0-meson composition of the 4π final state we calculated the acceptance in bins of invariant masses $m(\pi^+,\pi^-)$. It is, however, not sufficient to form a two dimensional weight matrix in $m(\pi_1^+,\pi_2^-)$, $m(\pi_3^+,\pi_4^-)$. The acceptance for constant $m(\pi_1^+,\pi_2^-)$, $m(\pi_3^+,\pi_4^-)$ still depends on the way the $\pi\pi$ mass distribution has been generated. This is a consequence of the "symmetrization" process for the amplitude of process (1). Because of the spin 0 nature of the pions one has to form a symmetric amplitude for the process $\gamma\gamma\to 4\pi$ as follows (in the special case when one or two ρ^0-mesons are formed):

$$A(\gamma\gamma\to 4\pi)\sim f_1(\pi_1^+\,\pi_2^-)\cdot f_2(\pi_3^+\,\pi_4^-)$$
$$+ f_1(\pi_1^+\,\pi_4^-)\cdot f_2(\pi_3^+\,\pi_2^-) \tag{2}$$

the functions f being either a Breit-Wigner amplitude or a phase space factor. In order to properly correct for acceptance losses, one has to calculate all four unlike-sign mass combinations for a measured event and multiply with a 4 dimensional weight matrix element (in $m(\pi^+,\pi^-)$). Using this method the acceptance is calculated free of assumptions concerning the composition into different f_1,f_2.

Apart from the mass distribution the acceptance also depends on the angular distributions of the production of the "ρ^0" and its decay. In a first step we tried to measure these distributions.

b) Production of the "ρ^0"

To arrive at an acceptance corrected distribution in $\cos\theta_\rho$ (θ_ρ=polar angle in the c.m. system with respect to the beam axis) we studied five different models for the mass dependence and the decay of the "ρ^0":

a) $\gamma\gamma\to\rho^0+\rho^0$ with $\sin^2\theta^H$ decay of the rhos,

b) $\gamma\gamma\to\rho^0+\rho^0$ with isotropic decay,

c) $\gamma\gamma\to\rho^0+2\pi$ with $\sin^2\theta^H$ decay of the ρ^0,

d) $\gamma\gamma\to\rho^0+2\pi$ with isotropic decay,

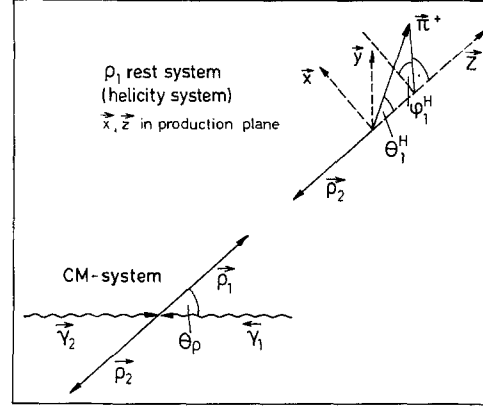e) $\gamma\gamma\to 4\pi$ according to phase space and isotropic decay.

Fig. 2. Schematic overview of the production and decay angles in the c.m.- and the helicity-system
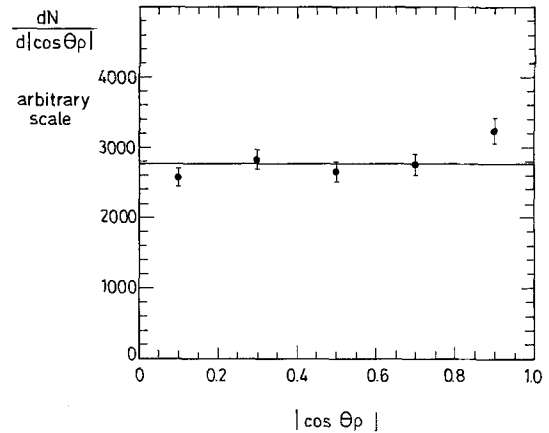

Fig. 3. The acceptance corrected distribution of the "ρ^0" production angle $\cos\theta_\rho$ in the c.m.-system. Events are selected in the c.m.-energy bin $1.3 < W_{\gamma\gamma} < 2.3$ GeV and $0.66 < m(\pi\pi) < 0.86$ GeV

Here θ^H is the polar angle of the decay π^+ in the rest system of the ρ^0, where the z-axis is chosen to be the negative direction of flight of the second "ρ^0" system (helicity system, see Fig. 2).

For the c.m. energy $W_{\gamma\gamma}$ the range 1.3 to 2.3 GeV was chosen where most of the events are concentrated. The Monte Carlo simulations were first done in bins of 200 MeV, and in a second step the weighted sums of the five energy bins were formed according to the measured numbers of real events in the different energy bins.

We arrive at the result that the $\cos\theta_\rho$-distribution is flat with only minor dependencies on the way the acceptance correction was done. Figure 3 shows this result for the correction method b.

c) Decay of the "ρ^0"

For the study of the decay distribution of a "ρ^0", the data were acceptance corrected using an isotro-
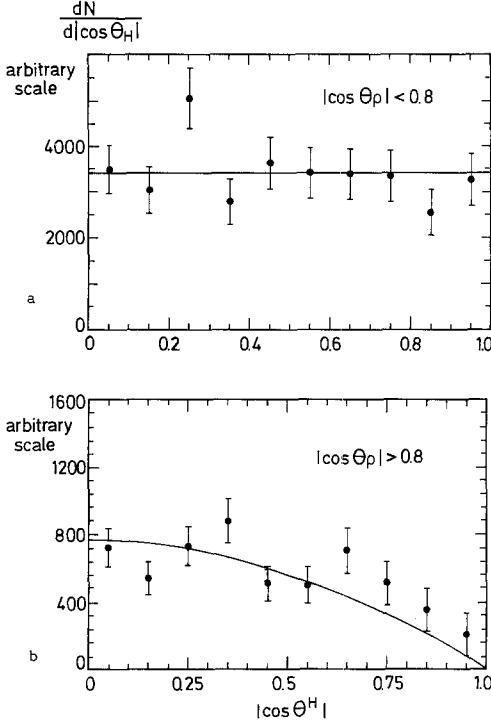
Fig. 4. a The acceptance corrected distribution of the decay π^+ from a "ρ^0", $\cos\theta^H$, for the central range of the production angle $|\cos\theta_\rho| < 0.8$. θ^H is the polar angle of the π^+ in the helicity system. **b** The analogue distribution for the range of forward produced rhos $|\cos\theta_\rho| > 0.8$

pic production of a ρ^0 or 2π system respectively. For the mass distribution all three models $\rho\rho$, $\rho 2\pi$ and 4π were tried. Here it was found, again independent of the detailed model, that one can distinguish two different regions: For $|\cos\theta_\rho| < 0.8$ the distribution in $\cos\theta^H$ is consistent with an isotropic decay of a "ρ^0" system, whereas for the forward region $|\cos\theta_\rho| > 0.8$ a flat distribution in $\cos\theta^H$ gives unacceptable fits, while a $\sin^2\theta^H$ distribution yields a perfectly good fit*. Figure 4 shows the result for the decay angular distribution. The acceptance correction in this case was done with the model $\gamma\gamma \to \rho^0\rho^0$.

In order to be sensitive to the ρ^0-mesons in the data sample all these studies on angular dependencies were made for events inside an invariant mass band of ± 100 MeV around the ρ^0-mass.

d) Monte Carlo Simulation

The acceptance correction for the measured angular distributions (Sects. 3b and 3c) was done using

---

* Fit quality (confidence level) for decay models:

$|\cos\theta_\rho| < 0.8$ and isotropic decay:

C.L. $= 26\%$, $\sin^2\theta$-decay: C.L. $< 0.1\%$;

$|\cos\theta_\rho| > 0.8$ and isotropic decay:

C.L. $= 0.7\%$, $\sin^2\theta$-decay: C.L. $= 9.1\%$

Monte Carlo simulations of the experiment described in detail in the following.

Let the measured uncorrected angular distribution in $\cos\theta_\rho$ (or $\cos\theta^H$ alternately) be called $df_M(\cos\tilde\theta)/d(\cos\tilde\theta)$ where we have added up all events within the following boundaries:

$1.3 < W_{\gamma\gamma} < 2.3$ GeV for the c.m. energy,

$0.25 < m(\pi\pi) < 1.5$ GeV for the invariant masses of the $m(\pi\pi)$-systems,

$-1 < \cos\theta_1^H$, $\cos\theta_2^H$ $(\cos\theta_\rho) < +1$ for the decay (production) angles,

$0 < \phi_1^H$, ϕ_2^H $(\phi_\rho) < 2\pi$ for the azimuths of the decay (production) angles.

The acceptance corrected angular distribution then is

$$\frac{df_A(\cos\tilde\theta)}{d(\cos\tilde\theta)} = \frac{df_M(\cos\tilde\theta)}{d(\cos\tilde\theta)} \cdot \frac{1}{A(\cos\tilde\theta)} \qquad (2)$$

where the acceptance correction $A(\cos\tilde\theta)$ has to be calculated as follows:

$$A(\cos\tilde\theta)$$
$$= \int d\mathbf{k}_1 \, d\mathbf{k}_2 \, d\mathbf{x} \cdot \sigma_{\gamma\gamma}(\mathbf{k}_1,\mathbf{k}_2) \cdot \frac{d\sigma(W_{\gamma\gamma},\mathbf{x})}{d\mathbf{x}} \cdot A(\mathbf{k}_1,\mathbf{k}_2,\mathbf{x})$$

$$\Big/ \int d\mathbf{k}_1 \, d\mathbf{k}_2 \, d\mathbf{x} \cdot \sigma_{\gamma\gamma}(\mathbf{k}_1,\mathbf{k}_2) \cdot \frac{d\sigma(W_{\gamma\gamma},\mathbf{x})}{d\mathbf{x}} \qquad (3)$$

with $\mathbf{k}_1, \mathbf{k}_2 =$ incoming photon momenta,

$\sigma_{\gamma\gamma} =$ function for the photon flux,

$\sigma(W_{\gamma\gamma},\mathbf{x}) =$ differential cross section for the process $\gamma\gamma \to 4\pi$,

$\mathbf{x} =$ vector of the kinematic variables $m(\pi\pi)$, $\cos\theta_1^H$, $\cos\theta_2^H$ $(\cos\theta_\rho)$, ϕ_1^H, $\phi_2^H(\phi_\rho)$.

The integration over $d\mathbf{k}_1$, $d\mathbf{k}_2$ has to be performed in such a way that the total c.m. energy varies between 1.3 and 2.3 GeV. The photon flux factors were computed according to [5].

The cross section $\sigma(W_{\gamma\gamma},\mathbf{x})$ can be factorised as follows:

$$\frac{d\sigma(W_{\gamma\gamma},\mathbf{x})}{d\mathbf{x}} \sim |g_1(\mathbf{x}) \cdot g_2(W_{\gamma\gamma})|^2. \qquad (4)$$

Here one has assumed that the dependence of the cross section on angles and $m(\pi\pi)$ does not change with the c.m. energy*. This factorization allows us to proceed for the integrations in the following way:

i) Calculation of the integral in the denominator by M.C.-generating events with a constant $g_2(W_{\gamma\gamma})$ inside a 200 MeV bin of $W_{\gamma\gamma}$ for the five different energy bins between 1.3 and 2.3 GeV.

---

* This has been studied to a certain extent and no such dependence was found (see p. 218)

ii) Calculation of the numerator integral inside the 200 MeV bands by subjecting each event to a full simulation of the experimental apparatus and analysis and keeping only the surviving events.

iii) Performing the integrations over the c.m. energy by forming weighted sums of the individual integrals where the weights are proportional to the total measured rates in the individual energy bins.

For the amplitude function $g_1(x)$ we used different formulae for the $\rho\rho$, $\rho 2\pi$ or 4π final states, resp. In the process $\gamma\gamma \to \rho\rho$ the production amplitude is described by two p-wave Breit-Wigner amplitudes. As stated earlier, we have to symmetrize the amplitude by using both combinations of the unlike-sign π's:

$$g_1(x) = BW(m(\pi_1^+\pi_2^-)) \cdot BW(m(\pi_3^+\pi_4^-))$$
$$\cdot W(\theta_\rho, \phi_\rho, \theta_1^H, \theta_2^H, \phi_1^H, \phi_2^H)$$
$$+ BW(m(\pi_1^+\pi_4^-)) \cdot BW(m(\pi_3^+\pi_2^-))$$
$$\cdot W(\theta_\rho', \phi_\rho', \theta_1^{H'}, \theta_2^{H'}, \phi_1^{H'}, \phi_2^{H'}) \tag{5}$$

where the Breit-Wigner functions are given by

$$BW(m) = \frac{\sqrt{M_\rho \cdot \Gamma}}{M_\rho^2 - m^2 - iM_\rho\Gamma} \tag{6}$$

with

$$\Gamma = \Gamma_\rho \left(\frac{p^*}{p_\rho^*}\right)^3 \cdot \frac{2p_\rho^{*2}}{p^{*2} + p_\rho^{*2}}.$$

The angles θ, ϕ are, respectively, the production, decay-angles for the first possibility of pairing the pions $m(\pi_1^+\pi_2^-)$, $m(\pi_3^+\pi_4^-)$, the angles θ', ϕ' the equivalent angles for the second possibility of the pairing $m(\pi_1^+\pi_4^-)$, $m(\pi_3^+\pi_2^-)$. The pion momentum in the $\pi\pi$ rest system is called p^* with $p_\rho^* = p^*$ for $m = m_\rho$. For the width and central mass of the ρ^0-meson we used $\Gamma_\rho = 155$ MeV and $m_\rho = 776$ MeV.

For the angular functions W, two different possibilities were used as described in Sect. 3b:

- $W = $ const
- $W = \sin\theta_1^H \cdot \sin\theta_2^H (\sin\theta_1^{H'} \cdot \sin\theta_2^{H'})$. $\tag{7}$

In case of the $\gamma \to \rho 2\pi$ amplitude the function $g_1(x)$ has to be written as follows:

$$g_1(x) = BW(m(\pi_1^+\pi_2^-)) \cdot PS_2(m(\pi_3^+\pi_4^-)) \cdot W(\theta_1^H)$$
$$+ BW(m(\pi_3^+\pi_4^-)) \cdot PS_2(m(\pi_1^+\pi_2^-)) \cdot W(\theta_2^H)$$
$$+ BW(m(\pi_1^+\pi_4^-)) \cdot PS_2(m(\pi_3^+\pi_2^-)) \cdot W(\theta_1^{H'})$$
$$+ BW(m(\pi_3^+\pi_2^-)) \cdot PS_2(m(\pi_1^+\pi_4^-)) \cdot W(\theta_2^{H'}). \tag{8}$$

Here the functions PS_2 are the two particle phase space functions in the variable $m(\pi\pi)$. In the case that the four pions do not form a resonance we

assume a phase space distribution of the pions with

$$g_1(x) = PS_4(m(\pi_1^+\pi_2^-),\ m(\pi_3^+\pi_4^-),\ m(\pi_1^+\pi_4^-),\ m(\pi_3^+\pi_2^-)).$$

This is the four particle phase space expressed in the invariant mass variables.

e) The Experimental Result

According to the results of the measurement of the angular distributions (see Sects. 3b and 3c), two different sets of weight matrices were formed:

- for $|\cos\theta_\rho| < 0.8$ the weight matrices were computed with a flat distribution in the decay angle $\theta_{1,2}^H$ of the "ρ^0",
- for $|\cos\theta_\rho| > 0.8$ we used the $\sin^2\theta_{1,2}^H$-distribution for the acceptance computation.

As stated in Sect. 3a, our method is independent of the choice of the mass distribution of the generated Monte Carlo data within our restriction of $\rho\rho$, $\rho 2\pi$ or 4π (PS) formation. To increase the Monte Carlo statistics for the acceptance computation and to get good coverage of the entire $m(\pi\pi)$ region we used, in the first set, Monte Carlo data which were produced according to all 3 models with isotropic decay, while, in the second set, only events from the $\gamma\gamma \to \rho\rho$ hypothesis with $\sin^2\theta^H$-decay were used. Two different choices for the widths of the invariant mass bins were tried for computing the weight matrices:

$$-\Delta m(\pi\pi) = 250 \text{ MeV},$$

$$-\Delta m(\pi\pi) = 100 \text{ MeV}.$$

No systematic differences outside the statistical error were discovered, so we used the bin width $\Delta m(\pi\pi) = 250$ MeV since fewer Monte Carlo events were needed to make the statistical error in the corrections negligible in this case. The experimental data and the Monte Carlo events were distributed into 7 equal $W_{\gamma\gamma}$-bins between 1.1 and 2.5 GeV. The calculation of the weight matrices was done equivalently to the procedure described in Sect. 3d (3), except that the integration over $m(\pi\pi)$ was done in 250 MeV wide bins and over $W_{\gamma\gamma}$ in 200 MeV bins. The cross section in the individual bins was calculated by adding the appropriate weight matrix elements and by multiplying with a factor determined by the number of incoming gammas in the individual $W_{\gamma\gamma}$-bins. The average acceptances for the different $W_{\gamma\gamma}$ are listed in Table 1.

Table 1. Acceptances for the different $W_{\gamma\gamma}$-ranges

$W_{\gamma\gamma}$ [GeV]	1.1 -1.3	1.3 -1.5	1.5 -1.7	1.7 -1.9	1.9 -2.1	2.1 -2.3	2.3 -2.5
accept. [%]	3.8	6.8	9.3	10.8	11.7	11.5	8.5

Overall corrections were applied as follows:

	correction factor
– corrections due to losses in a fast selection program (losses occurred mainly due to a high number of cathode hits)	1.20 ± 0.04
– losses in the track finding program which were not simulated in the Monte Carlo studies	1.28 ± 0.06
– losses in the trigger due to efficiency problems in the chambers	1.05 ± 0.02
– losses due to additional accidental tracks inside the vertex ranges	1.03 ± 0.01
– losses due to wrong momentum determination	1.02 ± 0.01
– events outside the cut at $p_\perp^t = 0.12$ GeV	1.14 ± 0.02
– background under the peak at small $p_\perp^t$	0.91 ± 0.02
– luminosity	1.00 ± 0.02

With these corrections we arrive at a total correction factor of 1.76 ± 0.11. The cross section in bins of $W_{\gamma\gamma}$ is listed in Table 2 and plotted in Fig. 5.

Table 2. The total cross section $\gamma\gamma \to \pi^+\pi^+\pi^-\pi^-$ as a function of the energy of the $\gamma\gamma$-system $W_{\gamma\gamma}$

$W_{\gamma\gamma}$ [GeV]	Cross Section [nanobarn]
1.1–1.3	98 ± 16
1.3–1.5	201 ± 20
1.5–1.7	182 ± 18
1.7–1.9	157 ± 16
1.9–2.1	120 ± 19
2.1–2.3	67 ± 11
2.3–2.5	50 ± 14

Here only the statistical errors are given. An additional correction factor of about 1.1 due to the fact that the incoming gammas possess a finite mass squared of 0.05 GeV^2 was not taken into account. This factor arises if one introduces a ρ-pole form factor $F = (1 + Q^2/M_\rho^2)^{-1}$ which suppresses the production process compared to that with real photons. An additional systematic error due to uncertainties in the acceptance was estimated to be 8%, so that the overall systematic error is found to be 10%.

We see a sharp fall off above 1.5 GeV. Neither the absolute magnitude nor the energy dependence can be easily explained by a simple VDM-model. Simple VDM-considerations predict for the process $\gamma\gamma \to \rho\rho$ only 5–10 nb in this energy range [1], while calculations by G. Alexander et al. [7] explain, on the basis of factorization used explicitly for low energies,
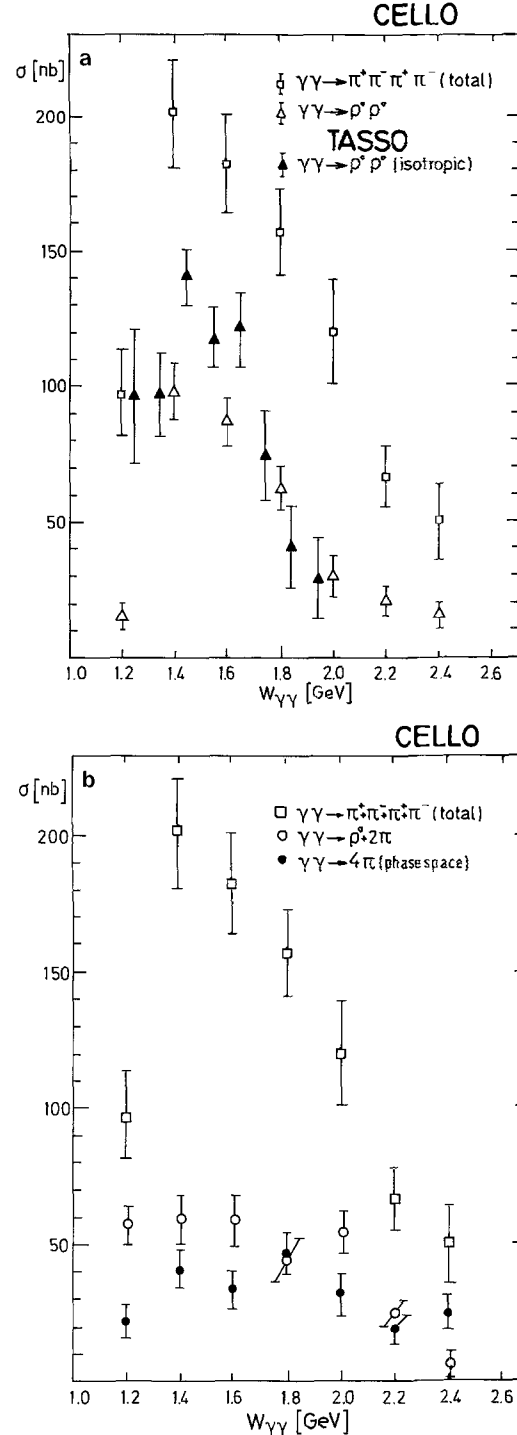

Fig. 5. a The total cross section for the process $\gamma\gamma \to \pi^+\pi^-\pi^+\pi^-$ as a function of the c.m.-energy. Included are the distributions for $\gamma\gamma \to \rho^0\rho^0$ and a comparison with TASSO [1] for their "isotropic model". **b** The total cross section and the components $\gamma\gamma \to \rho^0 2\pi$ and $\gamma\gamma \to 4\pi$ (PS) as a function of $W_{\gamma\gamma}$

most of the cross section and also the sharp decay of the cross section at higher $W_{\gamma\gamma}$.

There is one earlier publication of the total $\gamma\gamma \to 4\pi$ cross section by the MARK II group at
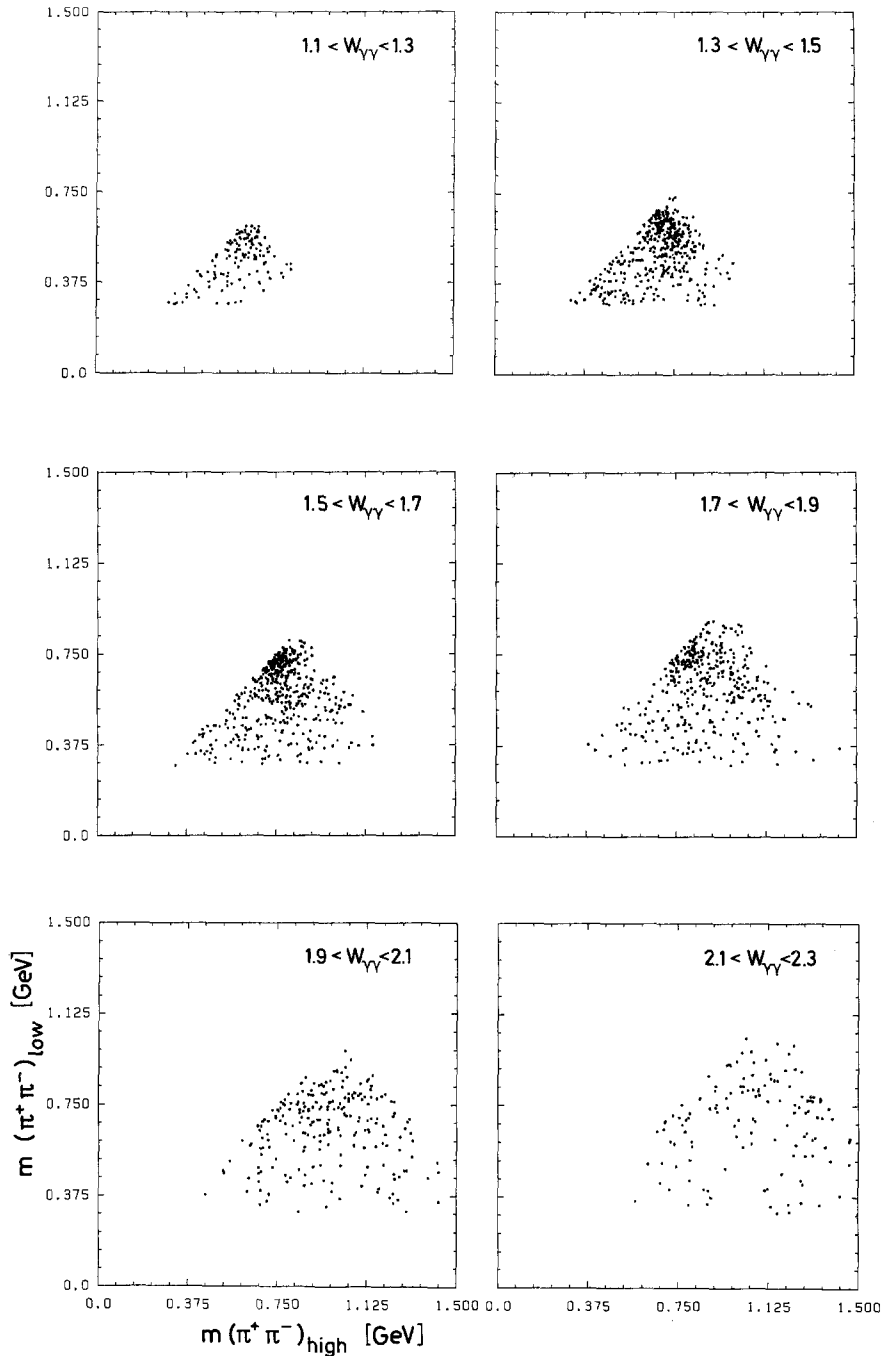
Fig. 6. The scatter plots for $m(\pi^+\pi^-)_{\text{low}}$ versus $m(\pi^+\pi^-)_{\text{high}}$ for different c.m.-energy bins. There are two entries per event

SPEAR [2] with results almost a factor two lower than here. The difference is, to a large extent, due to the different methods of the acceptance calculation. Those authors calculated the acceptance only for $\gamma\gamma \to \rho\rho$ implying that this channel already saturates the 4π cross section. There is however reasonable agreement of this experiment with the TASSO-1982 data [1] if one adds up their different contributions for $\rho\rho$, $\rho 2\pi$ and 4π (PS).

4. The Relative Contributions of $\rho\rho$, $\rho 2\pi$ and 4π (PS) to the 4π-Cross Section

a) Description of the Method

For this analysis we plot the invariant masses $m(\pi_1^+\pi_2^-)$, $m(\pi_3^+\pi_4^-)$ and $m(\pi_1^+\pi_4^-)$, $m(\pi_3^+\pi_2^-)$ in a common scatter plot (2 entries per event) with the higher mass always plotted horizontally. Figure 6 shows the

scatter plots for the different $W_{\gamma\gamma}$-bins. There is obviously a strong ρ^0-signal in the energy bins 1.3 to 1.9 GeV. For the determination of the relative $\rho\rho$, $\rho 2\pi$ and 4π (PS) contributions these distributions were fitted to Monte Carlo data, which were produced as described in Sect. 3d. Again we have used the result of the angular analysis:

For the "ρ^0"-decay a flat dependence in $\cos\theta^H$ was used for $|\cos\theta_\rho| < 0.8$, and a $\sin^2\theta^H$ distribution for $|\cos\theta_\rho| > 0.8$. The production of the "ρ^0" in the overall c.m. system was isotropically distributed in agreement with the data.

In the fitting procedure, a maximum likelihood method for Poisson distributed data was used. Particular care was given to the calculation of χ^2 for the best fits. Neighbouring bins with a content lower than five were combined to give a content greater than five. Even if the fit is not performed by demanding the minimum of χ^2, one generally assumes that for a fit function describing well the measured data, the value of $\sqrt{2\chi^2}$ will have a gaussian distribution with unit standard deviation about a mean value of $\sqrt{2F-1}$ (F = number of degrees of freedom). The χ^2-probability or confidence level (C.L.) was determined from χ^2 and F. A confidence level of lower than 5% generally indicates an unacceptable fit. Fits were performed to individual models and all combinations of $\rho\rho$, $\rho 2\pi$ and 4π.

We studied in particular the following:

- Comparison of fits made to both sets of data A and B as described in Sect. 2, using the important feature that CELLO can recognize photons in almost the full solid angle.

- One gains additional information, if fits are done simultaneously to the scatter plot of the unlike-sign combinations of the 4π *and* to the $\pi^+\pi^+$ versus $\pi^-\pi^-$-distributions. For a good fit we have to demand not only an acceptable C.L. but also a reasonable agreement of the fit and data integrals for the individual plots.

- Fits also were constrained to the region above 540 MeV with only unlike-sign combinations, where the $\rho\rho$ and $\rho 2\pi$ contributions are particularly different.

- Fits were done in individual 200 MeV-bins and also, for better statistical accuracy, in the $W_{\gamma\gamma}$-range where most of the data are concentrated (1.3–1.9 GeV). The latter has the disadvantage, however, that one combines data from an energy regime where the shape of the ρ-signal is rapidly varying with $W_{\gamma\gamma}$ due to the kinematical threshold for $\rho\rho$-production. For this case the Monte Carlo events, which were produced in 200 MeV bins, were added up using weights proportional to the measured total 4π rates in the individual energy bins.

Table 3. Fit quality for one, two and three component fits computed for the c.m.-energy range $1.3 < W_{\gamma\gamma} < 1.9$ GeV (common fit to like-sign and unlike-sign distributions)

Fit function	Confidence level [%]
$\rho\rho$	<1
$\rho 2\pi$	5
4π	<1
$\rho\rho + \rho 2\pi$	7
$\rho\rho + 4\pi$	8
$\rho 2\pi + 4\pi$	7
$\rho\rho + \rho 2\pi + 4\pi$	50

b) Fits in the Energy bin $1.3 < W_{\gamma\gamma} < 1.9$ GeV

The first important result is the following: The 3 component fit, including $\rho\rho$, $\rho 2\pi$ and 4π (PS), to the "clean" data sample B, simultaneoulsy fitted to unlike-sign and like-sign distributions, gives a C.L. = 63%, proving that our ansatz describes the data very satisfactorily. Here we included all events from threshold to an invariant mass of $m(\pi\pi) = 1,500$ MeV. The same fit for the dataset A is somewhat poorer (C.L. = 17%), but the fit quality improves considerably (C.L. = 50%) if we raise the lower $m(\pi\pi)$ cut slightly from threshold to 330 MeV. In the following we therefore use data sample A with the higher threshold since it has about 30% more statistical accuracy than dataset B.

In Table 3, we give the results for the fits to the single amplitudes and all combinations of them. The result can be interpreted as follows:

- The single amplitudes give fits which are unacceptable for pure $\rho\rho$ and pure 4π (PS) models, the fit is barely acceptable for pure $\rho 2\pi$.

- The twofold combinations give fits which are barely acceptable, with C.L. of 7–8%.

- A good fit and a dramatic improvement of the fit quality is only achieved by including all three components.

c) Fits in bins of $\Delta W_{\gamma\gamma} = 200$ MeV

The statistical accuracy is not considered sufficient to reach conclusions about different compositions in the energy ranges $1.1 < W_{\gamma\gamma} < 1.3$ and $2.1 < W_{\gamma\gamma} < 2.5$ GeV. Results for the other energy ranges are given in Tables 4 and 5. We tested in particular if the common fit to unlike-sign and like-sign distributions gives good agreement for the individual integrals and also the behaviour for fitting only unlike-sign plots above 540 MeV, were the 4π (PS) contribution is not so important and the $\rho\rho$ and $\rho 2\pi$ models show the greatest difference (the "ρ^0"-peak is much wider for $\rho 2\pi$ than for $\rho\rho$). In general

Table 4. Fit quality (confidence levels and integrals to unlike-sign distributions) for two and three component fits, including and excluding the $\rho\rho$ and $\rho 2\pi$ components, for individual 200 MeV c.m.-energy bins (common fit to like-sign and unlike-sign $m(\pi\pi)$--distributions)

$W_{\gamma\gamma}$ [GeV]	$\rho\rho+4\pi$ (PS)		$\rho 2\pi+4\pi$ (PS)		$\rho\rho+\rho 2\pi+$ 4π (PS)		
	C.L. [%]	∫Fit	C.L. [%]	∫Fit	C.L. [%]	∫Fit	∫Data
1.3–1.5	1.5	427	<1	360	14	427	426
1.5–1.7	38	412	15	360	29	413	412
1.7–1.9	50	366	3.5	312	33	367	364
1.9–2.1	<1	198	5	182	8	198	201

Table 5. Fit quality (confidence levels) for two and three component fits, including and excluding the $\rho\rho$ and $\rho 2\pi$ components, for individual 200 MeV c.m.-energy bins (fits only to unlike-sign $m(\pi\pi)$-distributions for $m(\pi\pi) > 540$ MeV)

$W_{\gamma\gamma}$ [GeV]	$\rho\rho+4\pi$ (PS) C.L. [%]	$\rho 2\pi+4\pi$ (PS) C.L. [%]	$\rho\rho+\rho 2\pi+4\pi$ (PS) C.L. [%]
1.3–1.5	4	18	15
1.5–1.7	4	35	40
1.7–1.9	<0.01	2	3
1.9–2.1	70	60	75

one gets for some energy bins and some single models or twofold combinations reasonable fits if one tests the χ^2 alone. However, due to the smaller statistical accuracy, the fitting procedure combines more bins in the less populated areas in order to reach at least five events in the bin to be fitted. This effect tends to average out the differences.

Though we find acceptable χ^2 for some fits, also many problems occur for cases with only one or two amplitudes, which are listed below:

i) Simultaneous fit to unlike-sign and like-sign distributions

$1.3 < W_{\gamma\gamma} < 1.5$ GeV

model: $\rho\rho+4\pi$,	fit quality: C.L. = 1.5 % integral comparison: difference of 2 std. dev.
model: $\rho 2\pi+4\pi$,	fit quality: C.L. < 1 % integral comparison: difference of 2 std. dev.
model: $\rho\rho+\rho 2\pi+4\pi$,	fit quality: C.L. = 14 % integral comparison: perfect agreement

$1.5 < W_{\gamma\gamma} < 1.7$ GeV *and* $1.7 < W_{\gamma\gamma} < 1.9$ GeV

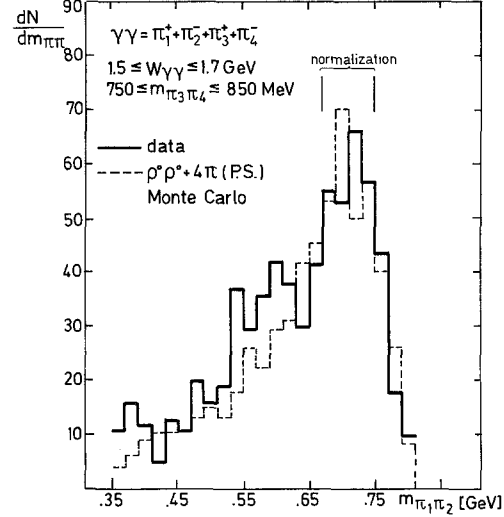|	
model: $\rho 2\pi+4\pi$,	fit quality: acceptable integral comparison: difference of 2 std. dev.

Fig. 7. The projection of events in the $m(\pi\pi)$ scatter plot for $1.5 < W_{\gamma\gamma} < 1.7$ GeV onto the horizontal axis for $0.75 < m(\pi\pi)_{high} < 0.85$ GeV (full histogram) compared to the Monte Carlo produced distribution for $\rho\rho+4\pi$ from the fit to the data (dashed histogram). The M.C. produced histogram is normalized to the four highest bins of the data histogram

$1.9 < W_{\gamma\gamma} < 2.1$ GeV

model: $\rho\rho+4\pi$,	fit quality: C.L. < 1 % (χ^2/D.F. = 147/92)
model: $\rho\rho+\rho 2\pi+4\pi$,	fit quality: C.L. = 8 % (χ^2/D.F. = 112/92).

Although the fit quality for the 3 component fit in this specific $W_{\gamma\gamma}$-range is still somewhat poor, the improvement by including the $\rho 2\pi$ component is remarkable.

ii) Fits to unlike-sign distributions for $m(\pi\pi) > 540$ MeV

$1.5 < W_{\gamma\gamma} < 1.7$ GeV

model: $\rho\rho+4\pi$,	fit quality: C.L. = 4 %
model: $\rho\rho+\rho 2\pi+4\pi$,	fit quality: C.L. = 40 %.

Since this is the highest populated energy bin, this result is considered as very significant for the test of the presence of the $\rho 2\pi$ amplitude. For an illumination of this result we show in Fig. 7 the projection of the data in the $m(\pi\pi)$-scatter plot on to the axis of the lower $m(\pi\pi)$-combinations for the $m(\pi\pi)$-range $750 < m(\pi\pi) < 850$ MeV in the higher $m(\pi\pi)$-combination. Also shown are the Monte Carlo data for $\rho\rho+4\pi$ normalized to the four bins around the ρ^0-peak. It is clearly seen that the $\rho\rho+4\pi$ curve has a smaller width than the data and is bound to give a bad fit.

Table 6. Fit results for the decomposition of the final state into $\rho\rho$, $\rho 2\pi$ and 4π (PS) for the three component fit using two wide $W_{\gamma\gamma}$-bins (common fit to like-sign and unlike-sign $m(\pi\pi)$-distributions)

$W_{\gamma\gamma}$ [GeV]	$\rho\rho$ [%]	$\rho 2\pi$ [%]	4π (PS) [%]
1.3–1.9	39±4	33±4	28±4
1.9–2.5	24±5	42±6	34±5

correlation coefficients $\rho_{12} = -0.63$, $\rho_{23} = -0.46$,
(for 1.3–1.9 GeV): $\rho_{13} = -0.15$

Table 7. Fit results for the decomposition of the final state into $\rho\rho$, $\rho 2\pi$ and 4π (PS) for the three component fit using small $W_{\gamma\gamma}$-bins (common fit to like-sign and unlike-sign $m(\pi\pi)$-distributions)

$W_{\gamma\gamma}$ [GeV]	$\rho\rho$ [%]	$\rho 2\pi$ [%]	4π (PS) [%]
1.1–1.3	14± 5	62± 7	24± 6
1.3–1.5	48± 5	31± 5	21± 4
1.5–1.7	47± 5	34± 5	19± 4
1.7–1.9	39± 5	30± 5	31± 4
1.9–2.1	24± 6	48± 7	28± 6
2.1–2.3	29± 7	40± 8	31± 7
2.3–2.5	29±11	17±11	54±12

$1.7 < W_{\gamma\gamma} < 1.9$ GeV

model: $\rho\rho + 4\pi$,   fit quality:
   C.L. < 1 % (χ^2/D.F. = 131/75)

model: $\rho\rho + \rho 2\pi + 4\pi$,   fit quality:
   C.L. = 3 % (χ^2/D.F. = 100/75).

Even if the 3 component fit in this restricted range is somewhat poor, the considerable change in χ^2 by including the $\rho 2\pi$ amplitude is important.

d) Results for the Decomposition of the Final State Into $\rho\rho$, $\rho 2\pi$ and 4π (PS)

We conclude from the fit studies that only the three component fit gives adequate fits to the data, independent of the fit region, and gives good agreement of the unlike-sign distribution integrals (data and fit) in all cases. The improvement of the confidence level for the combined energy data is much better than expected only by adding one more fit parameter.

We present the numerical results of our 3 component fits to the unlike- and like-sign distributions in two different forms. First we have divided up the energy range into two parts: For $1.3 < W_{\gamma\gamma} < 1.9$ GeV there appears a clear ρ-signal in the $m(\pi\pi)$-spectrum, for 1.9–2.5 GeV the ρ-signal is not apparent to the eye. We performed the 3 component fits separately in both energy ranges. The results are given in Table 6. We see that only about 40% in the highest populated energy range $1.3 < W_{\gamma\gamma} < 1.9$ GeV is due to $\gamma\gamma \to \rho\rho$ which is somewhat in contradiction to earlier published results [1, 2]. These authors found that the data are largely consistent with $\gamma\gamma \to \rho\rho$ plus a small 4π (PS) background*.

The errors given in Table 6 are the standard deviations given by the fitting procedure (diagonal elements of the error matrix). We also give the correlation coefficients ρ_{ij} which, by definition, are restricted to $-1 < \rho_{ij} < +1$. The coefficients show a rather large correlation between $\rho\rho$ and $\rho 2\pi$, a

small one between $\rho\rho$ and 4π and an intermediate one for $\rho 2\pi$ and 4π. Because of these correlations the errors given in the table cannot be taken for the significance of a specific amplitude.

Secondly, we performed the 3 component fit for the individual energy bins including $1.1 < W_{\gamma\gamma} < 1.3$. The results are given in Table 7 and plotted in Fig. 5. The two methods agree fairly well in their results as far as the breakup of the 4π final state into the three different components is concerned. Also shown are the results for $\gamma\gamma \to \rho\rho$ from the TASSO collaboration [1] (isotropic production and decay of the ρ's). The difference for $W_{\gamma\gamma} < 1.7$ GeV can be explained by the fact that TASSO could describe their data below 1.7 GeV without the $\rho 2\pi$ contribution and included it only above this energy.

From the individual energy bin fits we conclude the following: The process $\gamma\gamma \to \rho\rho$ has a sharp onset at and even below the nominal threshold for $\rho\rho$-production. Taking into account that the available phase space below 1.7 GeV shrinks drastically, the variation of the responsible matrix element towards lower energies is very strong, suggesting that we see the tail of a resonance at 1.0–1.2 GeV. There have been several attempts to try to explain this behaviour with known or conjectured resonances [1, 3]. These attempts include explanations by excitation and decay into 4π of the $f(1,270)$ or the $\varepsilon(1,300)$, which fail to explain the high cross section which is measured. Other authors have tried to explain the $\rho\rho$-signal by formation and decay of a glueball state or by excitation of a 4 quark state [3]. Additional information concerning resonant behaviour has been added recently by the JADE-collaboration [8] who gave a preliminary upper limit for the $\rho^+\rho^-$ final state of 40 nb.

The relatively sharp fall off on the high energy side has been explained by G. Alexander et al. [7] as consistent with VDM and factorization performed at low energies.

The cross section for 4π phase space is consistent with a constant cross section above threshold,

---
* The TASSO collaboration [1], however, also found a sizeable $\rho 2\pi$ component in this energy range for their 6 parameter fit, in accordance with our data

whereas the $\rho\,2\pi$ process follows an intermediate behaviour between the other two.

5. Analysis of the Angular Distributions

a) The Production Angle of the "ρ^0"

In Sect. 3b, we briefly treated the angular distribution of a $\pi\pi$ pair ("ρ^0") in the overall c.m. system. More information can be gained from a moment analysis since specific resonances which decay into a $\rho\rho$ final state reveal their angular momentum structure when this analysis is performed.

The moments of the spherical harmonics are defined by

$$\langle Y_L^M \rangle = \int I(\theta, \phi) \cdot Y_L^M(\theta, \phi)\, d\Omega \tag{10}$$

where $I(\theta, \phi)$ are the acceptance corrected experimental decay distributions with θ, ϕ being, respectively, the polar, azimuthal decay angles. The moment analysis for the ρ-production was performed

using essentially the same Monte Carlo generation schemes for the acceptance correction as described previously, namely all three clear processes ($\rho\rho$, $\rho\,2\pi$, 4π) were generated separately, the first two with a homogeneous and a $\sin^2\theta_{1,2}^H$ decay of the ρ. For these different assumptions the moments were calculated up to $L=4$ in bins of different $W_{\gamma\gamma}$. There was essentially no difference in the behaviour of the different moment calculations as far as the different acceptance corrections were concerned. In Fig. 8, the moments are shown versus $W_{\gamma\gamma}$. Here we only used events with $m(\pi\pi)$ within ± 100 MeV of the ρ^0-mass. There is no single moment significantly different from zero and no systematic change with $W_{\gamma\gamma}$ is apparent. We conclude from this analysis that states of negative parity (0^-, 2^-) decaying into two ρ^0's do not play any significant role since they demand the presence of an $L=1$ or $L=3$ wave, which should give rise to non-zero moments for these cases, in agreement with the TASSO analysis [1].
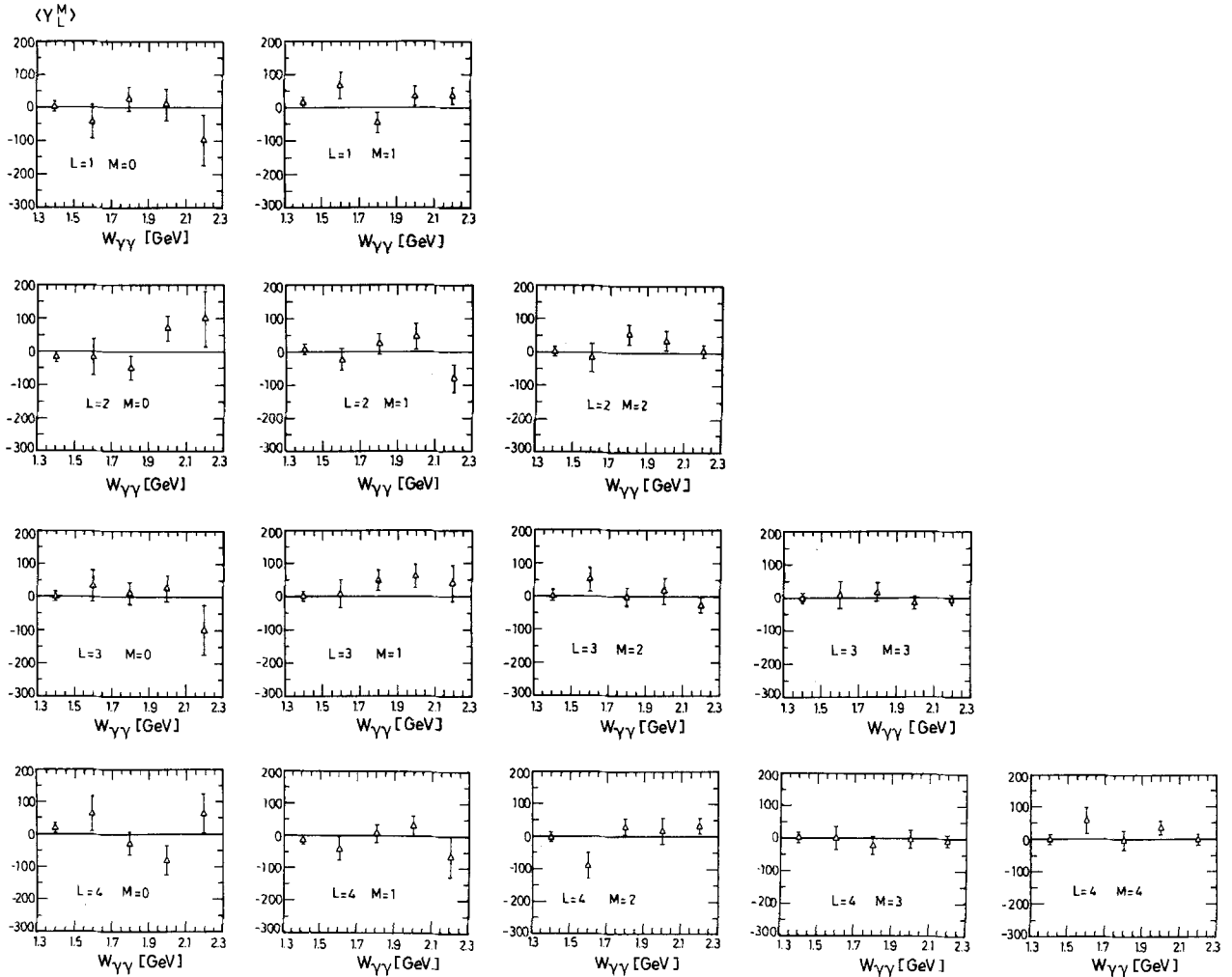

Fig. 8. The moments of the spherical harmonics for the production angles θ_ρ, ϕ_ρ in the c.m. system up to $L=4$ as a function of $W_{\gamma\gamma}$. Only events with $0.66 < m(\pi\pi) < 0.86$ GeV are selected

b) The Decay Angular Distribution

A moment analysis was also performed for the decay angular distribution. The acceptance correction was again done for the different model assumptions. Isotropic production of the "ρ^0" in the c.m. frame was applied in every case. Again the result is rather independent of the details of the acceptance correction. In Fig. 9 we show the moments as a function of $m(\pi\pi)$. Only the moments $L=2$ and $m=0, 2$ are different from zero as expected for the decay of a spin 1 particle like the ρ^0. It should be mentioned, however, that this behaviour persists to rather small $m(\pi\pi)$ masses which cannot be explained by a pure ρ^0-meson.

In the case of a spin 1 particle decaying into two spinless particles, the density matrix elements have simple relationships to the moments of the spherical harmonics. We present the density matrix elements for the energy range $1.3 < W_{\gamma\gamma} < 2.3$ GeV and for only

those events lying within ± 100 MeV of the ρ^0-mass in Table 8. The experimental result lies between the prediction for a random spin mixture and helicity conservation.

In a second step, we calculated the density matrix elements in 5 bins of $|\cos\theta_\rho|$. These results are plotted in Fig. 10, showing a dramatic change of the reaction dynamics above $|\cos\theta_\rho| \approx 0.6$, where ρ_{00} and ρ_{11} approach the limit for helicity conservation. This behaviour is expected if the ρ^0's are produced in the VDM picture as diffractively scattered virtual ρ^0-mesons. However, for pure helicity conservation also the ϕ-dependent element ρ_{1-1} should be zero, which is clearly not the case.

In a final step, we examined the behaviour of the density matrix elements with respect to $W_{\gamma\gamma}$ (Fig. 11), averaging over the production angle. There is no significant energy dependence visible; although, at very low energies, the data seem to fulfill the condition of arbitrary spin states best.
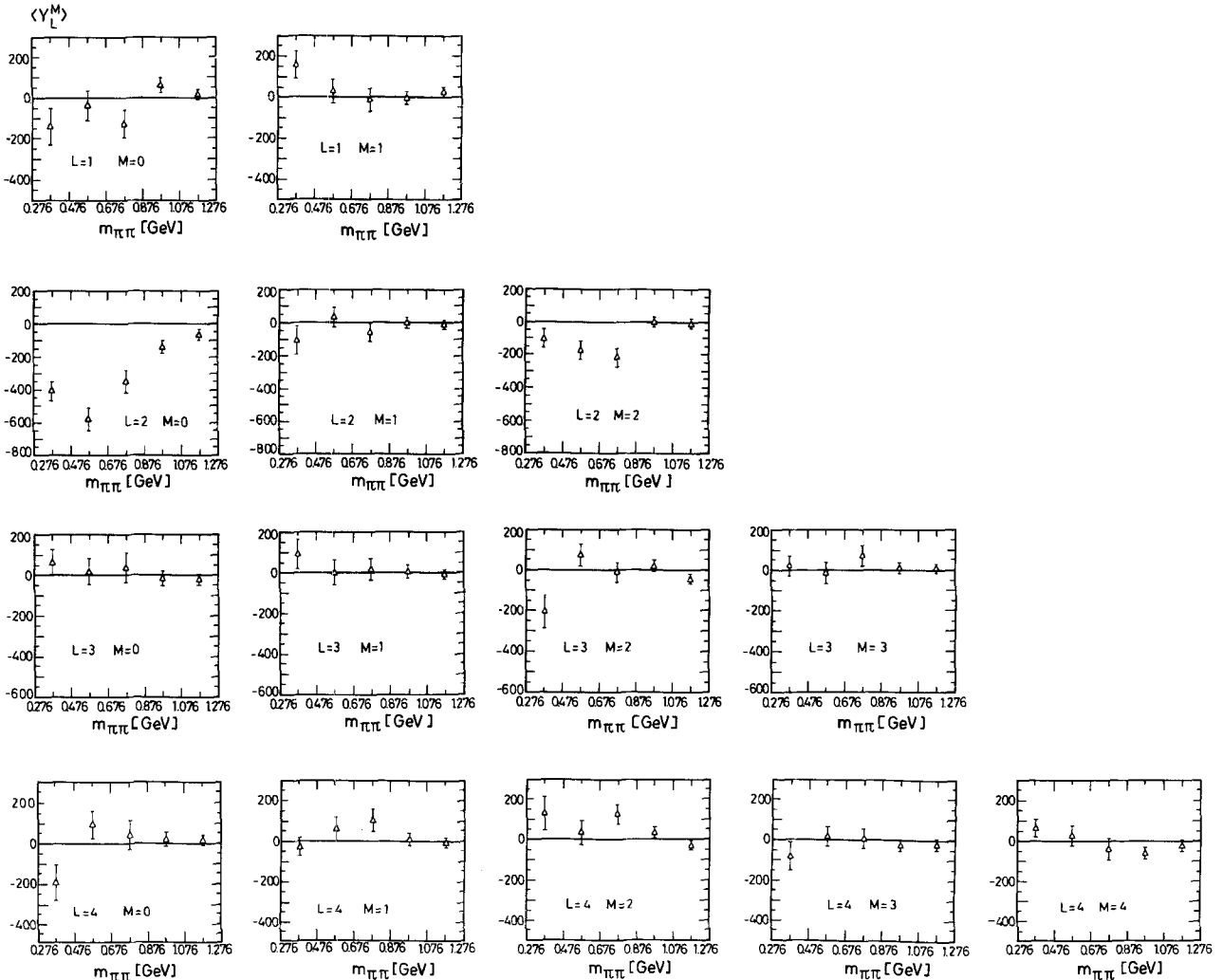

Fig. 9. The moments for the decay angle θ^H, ϕ^H of the decay π^+ of the "ρ^0" in the helicity system of the "ρ^0" up to $L=4$ as a function of the invariant $m(\pi\pi)$-mass. Events are selected as for Fig. 3
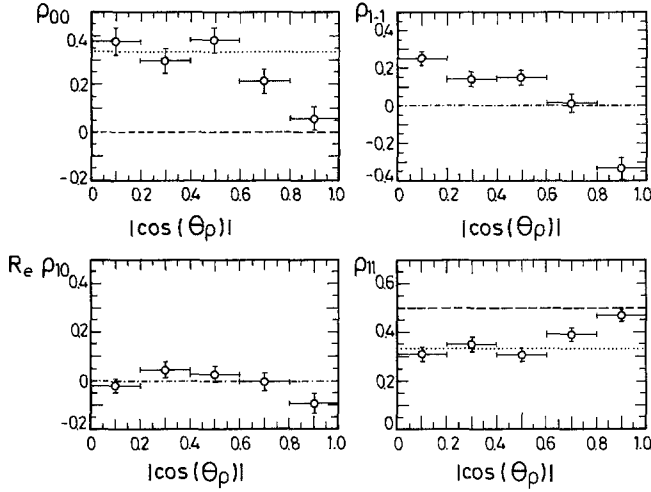
Fig. 10. The density matrix elements for the "ρ^0"-decay as a function of $\cos\theta_\rho$, the "ρ^0"-production angle. Events are selected as in Fig. 3. Prediction for ..... arbitrary helicity states; ----- helicity conservation
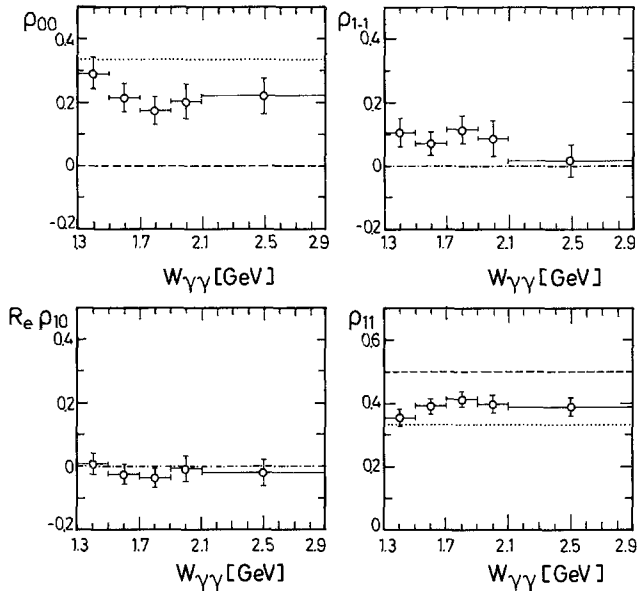

Fig. 11. The density matrix elements of the "ρ^0"-decay as a function of the c.m. energy $W_{\gamma\gamma}$, averaged over the production angle of the "ρ^0". Events are selected as in Fig. 8. Prediction for ..... arbitrary helicity states; ----- helicity conservation

Table 8. Density matrix elements in the c.m. energy range $1.3 < W_{\gamma\gamma} < 2.3$ GeV for the decay of a "ρ^0" state into $\pi^+\pi^-$. Only events with invariant masses $0.66 < m(\pi\pi) < 0.76$ GeV are accepted

Density matrix element	Experimental result	Prediction for	
		Random mixture of helicity states	Helicity conservation
ρ_{00}	0.22 ± 0.02	0.33	0
ρ_{1-1}	0.08 ± 0.02	0	0
$\mathrm{Re}\,\rho_{10}$	-0.02 ± 0.01	0	0
ρ_{11}	0.39 ± 0.01	0.33	0.5

6. Conclusions

We have determined the cross section for $\gamma\gamma \to \pi^+\pi^+\pi^-\pi^-$ in a way free of assumptions about the relative contributions from $\rho^0\rho^0$, $\rho^0 2\pi$ and 4π (uncorrelated phase space). We find a sharp onset above threshold and a rather high cross section of about 200 nb around $W_{\gamma\gamma} = 1.5$ GeV which consists to about 40% of $\rho^0\rho^0$ production with sizeable contributions from $\rho^0 2\pi$ and 4π (PS). The total cross section as well as the $\rho^0\rho^0$ content fall rather fast at higher c.m. energies. Attempts to explain this behaviour in terms of production of known resonances are not successful so far. The angular distributions do not show any significant structure pointing to resonance formation in the 4π-system. Only the ρ^0-meson is observed in the moment analysis. The decay distributions of the "ρ^0" for forward produced rhos are fairly consistent with helicity conservation of the produced rhos in accordance with the VDM picture.

References

1. TASSO Collab. R. Brandelik et al.: Phys. Lett. **97**B, 448 (1980); TASSO Collab. M. Althoff et al.: Z. Phys. C – Particles and Fields **16**, 13 (1982)
2. D.L. Burke et al.: Phys. Lett. **103**B, 153 (1981)
3. H. Goldberg, T. Weiler: Phys. Lett. **102**B, 63 (1981); J. Layssac, F.M. Renard: Clermont-Ferrand 1981, Proceedings. Gamma-Gamma Physics, 97; J. Layssac, F.M. Renard: Orsay 1981, Proceedings, Gamma-Gamma Physics, 87; R.M. Godbole, K.V.L. Sarma: Tate Instit. Preprint TIFR/TH/81-35; S. Minani: Lett. Nuovo Cimento **34**, 125 (1982); N.N. Achsov, S.A. Devyanin, G.N. Shestakov: Phys. Lett. **108**B, 134 (1982); Bing An Li, K.F. Liu: Phys. Lett. **118**B, 435 (1982); Erratum **124**B, 550 (1983)
4. CELLO Collab. H.-J. Behrend et al.: Phys. Scripta **23**, 610 (1981)
5. J.H. Field: Nucl. Phys. **B168**, 477 (1980); Erratum Nucl. Phys. **B167**, 545 (1980)
6. J.A.M. Vermaseren: Private communication; J. Smith, J.A.M. Vermaseren, G. Grammer Jr.: Phys. Rev. **D19**, 137 (1979)
7. G. Alexander et al.: Phys. Rev. **D26**, 1198 (1982)
8. H. Kolanoski: Aachen 1983, workshop on photon-photon interactions, Bonn-HE-83-9 (1983)